Food Chemistry: X 24 (2024) 101843

Contents lists available at ScienceDirect

Food Chemistry: X

journal homepage: www.sciencedirect.com/journal/food-chemistry-x

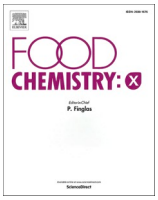

Cobalt oxyhydroxide nanoflakes enable ratiometric fluorescent assay of gallic acid

Chunlei Yang *, Guiju Xu, Chenghao Hou, Hongwei Zhang *

Institute of Food & Nutrition Science and Technology, Shandong Academy of Agricultural Sciences, Jinan 250100, PR China

ARTICLE INFO

Keywords:
CoOOH nanoflakes
Ratiometric fluorescence
Gallic acid detection
Fluorescent silicon nanoparticles

ABSTRACT

Gallic acid (GA) is widely used in beverages, food, and other fields as antioxidant. However, GA is slightly toxic and the accumulation of GA is harmful to human body. Therefore, it's vital to develop simple and sensitive detection methods for GA. In this work, a novel ratiometric fluorescent nanoprobe (named CoOOH/OPD/SiNPs) for the GA detection in different foods was designed and prepared. The fluorescence of silicon nanoparticles (SiNPs) at 443 nm would be quenched by cobalt oxyhydroxide (CoOOH) nanoflakes. *o*-phenylenediamine (OPD) would be oxidized to 2,3-diaminophenazine (DAP) by CoOOH nanoflakes that have peroxidase-like activity, which produces a new fluorescent peak at 556 nm. Meanwhile, SiNPs' fluorescence would be quenched through DAP due to inner filter effect (IFE). With the addition of GA, the reductive decomposition of CoOOH decreased DAP level, causing IFE being restrained. The concentration of GA indicates an excellent linear relationship with fluorescence ratio (F_{443}/F_{556}) in range of 0.4–12 μM ($R^2 = 0.9937$) with 0.16 μM detection limit. This nanoprobe is applied to GA detection in water, tea leaves, fruits and nut fruits, which would be expected to act as a portable device for complex substances analysis.

1. Introduction

Gallic acid (3,4,5-thihydroxybenzoic acid, GA), one of natural polyphenol compounds with hypotoxicity and straightforward chemical structure, widely exists in plants like gallnuts, fructus corni, sumac, rhubarb, oak bark, witch hazel, hops, grapes and tea (Boye et al., 2006; Stanković et al., 2017; X. Tan, Li, & Yang, 2020). As a strong antioxidant, gallic acid has lots of biological activities and pharmacological effects, for instance, antibacterial, anti-oxidation, anti-mutagenic and anti-tumor efficacy, etc. (Baghayeri, Amiri, Hasheminejad, & Mahdavi, 2018; Shahamirifard, Ghaedi, Razmi, & Hajati, 2018). Due to its three hydroxyl groups of GA chemical structure, it is well known as having high reducibility. GA makes extensive use of antioxidant in beverages, food, medicines and other fields (Niu, Pei, Ma, Yang, & Ma, 2022; Sekar et al., 2022). However, GA is slightly toxic and hard to biodegrade at low concentrations. The accumulation of gallic acid is bad for human health, which may cause several diseases, including dizziness, headache, fatigue and stomach upset, etc. (Chen et al., 2020; Liang et al., 2016; X. Wang, Tan, Wang, Wu, & Kong, 2019). Therefore, it is significance to establish sensitive and selective analytical methods for GA in food substances, which is critical to knowing their health benefits.

Currently, a variety of techniques have been developed for GA analysis, including high performance liquid chromatography (HPLC) (Švecová, Bordovská, Kalvachová, & Hájek, 2015), thin layer chromatography (TLC) (Dhalwal, Shinde, Biradar, & Mahadik, 2008), flow-injection chemiluminescence (S. Li et al., 2012), spectrophotometry (Dmitrienko, Medvedeva, Ivanov, Shpigun, & Zolotov, 2002), fluorescence spectroscopy (Pan et al., 2022), oscillating chemical reactions (Jiménez-Prieto, Silva, & Pérez-Bendito, 1996), capillary electrophoresis (H. X. Liu et al., 2014) and electrochemical methods(Badea et al., 2019). However, some of these techniques may suffer from limitations, such as requirement of sophisticated and costly instruments, time-consuming and not suitable for onsite field analysis. Due to its remarkable advantages, such as high sensitivity and selectivity, rapid response times and ease of applications, the fluorescent technique is a prospective way for gallic acid detection. Lots of fluorescent probes have been set up to detect gallic acid in recent years. Nevertheless, most fluorescent probes are based on a single signal, which is easily influenced by probe concentrations, environmental noises, excitation intensity, light source and measurement conditions (Huang et al., 2018). The ratiometric fluorescent probes have multi-fluorescence signals and one of them serves as a built-in calibration system, which can offer a background

* Corresponding authors.
E-mail addresses: chunlei_y@163.com (C. Yang), nkzhhw@163.com (H. Zhang).

https://doi.org/10.1016/j.fochx.2024.101843
Received 4 June 2024; Received in revised form 15 September 2024; Accepted 16 September 2024
Available online 17 September 2024

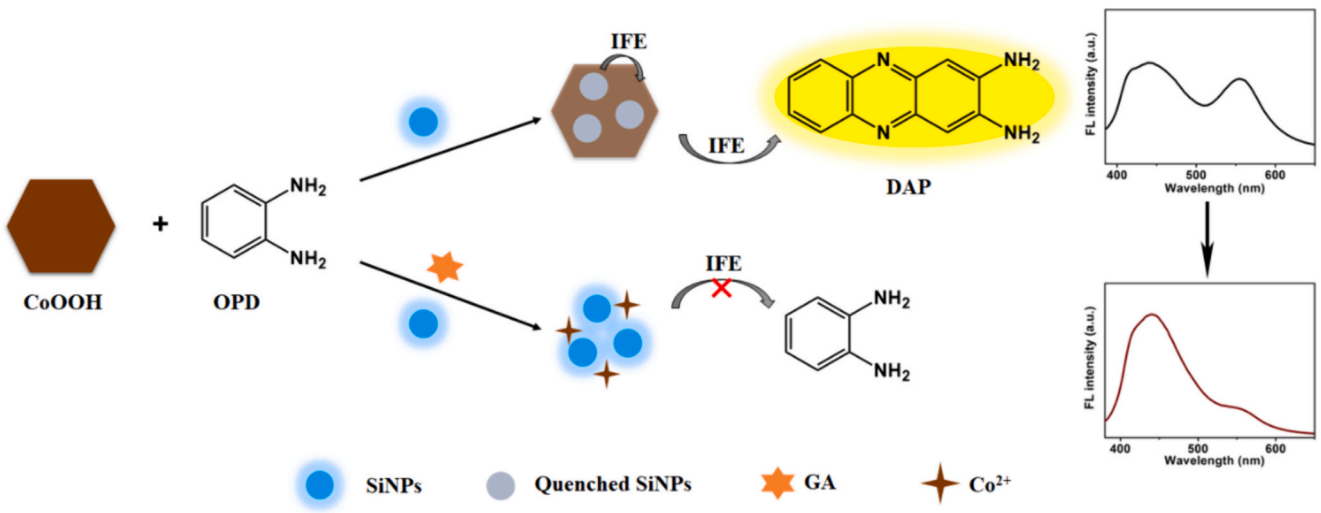

Scheme 1. Schematic depiction of fluorescent ratiometric nanoprobe (CoOOH/OPD/SiNPs) for gallic acid detection.

signal not influenced by light sources and environmental noise (M. Li et al., 2018; Pang & Liu, 2020; L. Wang et al., 2020; X. Xu et al., 2019). Therefore, it is great of significance to design a ratiometric fluorescent probe for gallic acid detection with low cost and simple operation.

Metal oxyhydroxide, a type of two-dimensional nanomaterials, have been attracted widespread attention because of its superior light absorption capability and large specific surface area (X.-P. Zhang, Zhao, Shu, & Wang, 2019). Cobalt oxyhydroxide (CoOOH) nanoflakes have been applied for the development of fluorescent sensors due to the fact that they have abundant hydroxyl functional groups on surface with favorable stability and dispersibility in aqueous medium (S. G. Liu et al., 2019; W. Xu et al., 2018). Fluorescent silicon nanoparticles (SiNPs) have some merits in applications of biological and optical biosensing, owing to their superior properties, including chemical inertness, stable photoluminescence, favorable biocompatibility, low toxicity and benign water solubility (Dou et al., 2017; Peng et al., 2014; X. Zhang et al., 2015). The preparation of SiNPs usually suffers from long reaction time, complex synthesis steps, low quantum yield or high reaction temperature (Xing et al., 2019). Thus, it is meaningful to develop SiNPs with good performance and explore for designing biosensors.

In the present work, we established a ratiometric fluorescence probe (denoted as CoOOH/OPD/SiNPs) for accurate detection of gallic acid (Scheme 1). The SiNPs with outstanding blue fluorescent emission serve as one of fluorescence signal. The CoOOH nanoflakes have simple preparation procedure, peroxidase-like activity and quenching capability. The CoOOH nanoflakes' absorption spectrum has a good overlap with emission spectrum of SiNPs. The fluorescence of SiNPs (443 nm) would be quenched by fluorescent inner filter effect (IFE). *o*-phenylenediamine (OPD) is catalytically oxidized to 2,3-diaminophenazine (DAP) by CoOOH nanoflakes, which generates a new fluorescent emission peak at 556 nm. Meanwhile, the fluorescence of SiNPs at 443 nm is quenched by DAP due to IFE. When the presence of GA, CoOOH nanoflakes would be reduced to Co^{2+}. The CoOOH nanoflakes are decomposed and decline DAP generation, which cause IFE being restrained. Thus, the fluorescent ratio at F_{443}/F_{556} regards as signal readout promotes the ratiometric fluorescence analysis of GA. This method could apply to determination of gallic acid in different tea leaves, fruits and nut fruits.

2. Experimental section

2.1. Materials and apparatus

Gallic acid (GA), (3-Aminopropyl) trimethoxysilane (APTMS, 97 %), cobalt chloride hexahydrate ($CoCl_2{\cdot}6H_2O$), KCl, $CaCl_2$, $MgCl_2$, $MnCl_2$, NaCl, sodium hypochlorite (NaClO), boric acid (H_3BO_3), sodium hydroxide (NaOH), 2,3-diaminophenazine (DAP), sucrose, phenol, catechol, salicylic acid, N-ethylmaleimide (NEM), arginine, glutamate, serine, sarcosine, glycine and leucine were obtained from Shanghai Macklin Biochemical Technology Co., Ltd. Acetic acid (HAc), phosphoric acid (H_3PO_4) and ethyl acetate were acquired from Sinopharm Chemical Reagent Co., Ltd. *o*-phenylenediamine (OPD) and glucose were purchased from Shanghai Aladdin Biochemical Techonology Co., Ltd.

Fluorescence spectra were recorded by F-7000 fluorescence spectrophotometer (Hitachi, Japan). Fluorescence lifetime curves were measured by FLS1000 steady state and transient state fluorescence spectrometer (Edinburgh, UK). The UV–vis absorption spectra were measured by TU-1901 double-beam spectrophotometer (Purkinje, Beijing). Scanning electron microscopy (SEM) and transmission electron microscopy (TEM) images were acquired by MIRA LMS (TESCAN, Czech) and Tecnai F20 (FEI, USA), respectively. X-ray photoelectron spectroscopy (XPS) spectra were measured by K-Alpha (Thermo Scientific, USA). X-ray diffraction (XRD) patterns were acquired by X-ray diffractometer (Panalytical Empyrean, Holland). Fourier-transform infrared (FT-IR) spectra were obtained with Nicolet iS20 spectrometer (Thermo Scientific, USA). The zeta potentials and sizes of prepared materials were measured by Malvern Zetasizer Nano ZS90 (Malvern, UK).

2.2. Preparation of fluorescent silicon nanoparticles

Fluorescent silicon nanoparticles (SiNPs) were carried out according to our previous work with further modification (Yang et al., 2021). The synthetic procedure was as follows: 30 mL of ultrapure water and 3.75 mL of APTMS stirred vigorously until mixed well. Afterwards, it was heated in a 50 mL autoclave for 2 h at 200 °C using hydrothermal method. After cooling to room temperature, purification steps were as follows: the SiNPs were collected and stirred with excess ethyl acetate. Stand for some time until the phase separated. The purified SiNPs of bottom aqueous phase were collected for further use.

2.3. Synthesis of CoOOH nanoflakes

The CoOOH nanoflakes were synthesized referring to previously literatures with minor modifications (Wu et al., 2019). Briefly, 300 μL of NaOH solution (1 M) was added to 10 mL of $CoCl_2{\cdot}6H_2O$ (10 mM) solution followed by ultrasonication for 5 min. Then, the mixture was

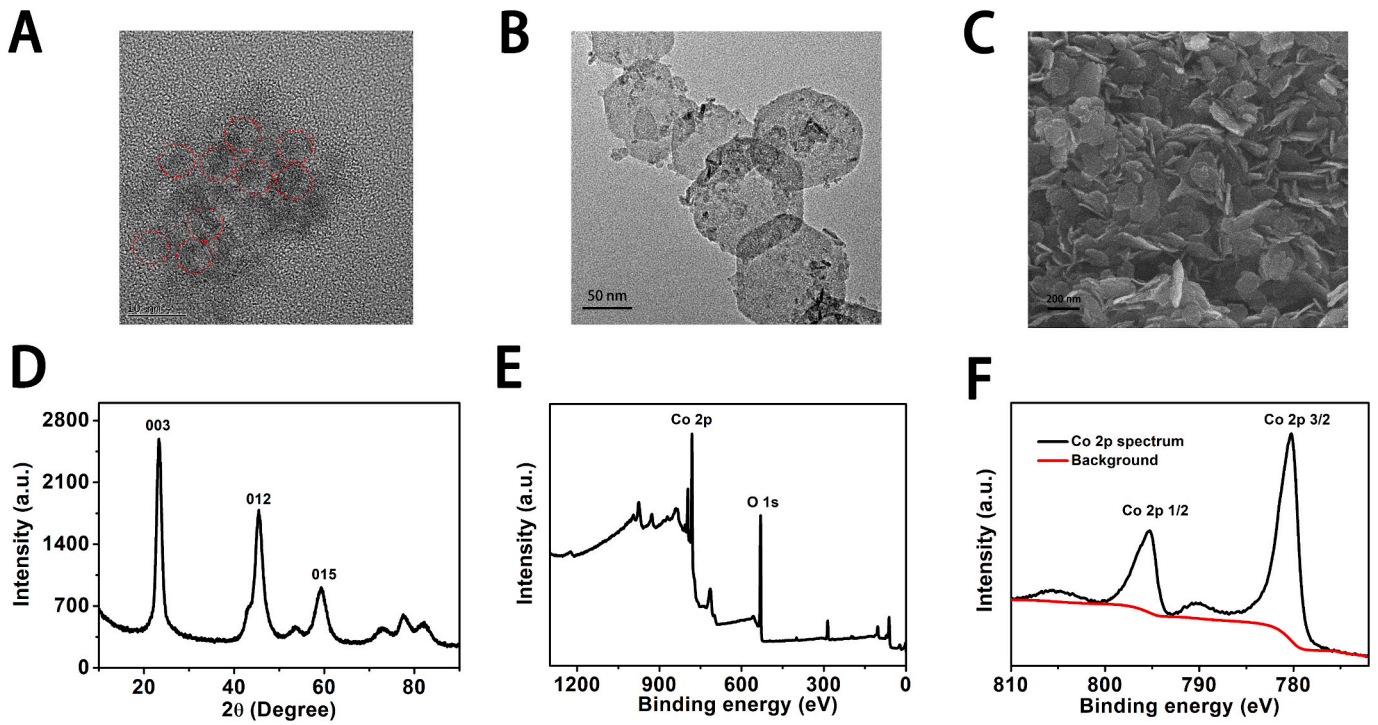

Fig. 1. TEM images of (A) SiNPs, (B) CoOOH nanoflakes, (C) SEM image of CoOOH nanoflakes, (D) XRD pattern and (E) XPS full spectrum of CoOOH, (F) High resolution Co 2p region of XPS for CoOOH.

collected by centrifuging (12,000 rpm, 10 min). Subsequently, acquired precipitate was re-dispersed in 10 mL water. 500 μL of NaClO (0.9 M) was dripped into the mixture with ultrasonication for 20 min. Next, the mixed solution was centrifuged and washed with ultrapure water. Finally, the product was dried with 60 °C.

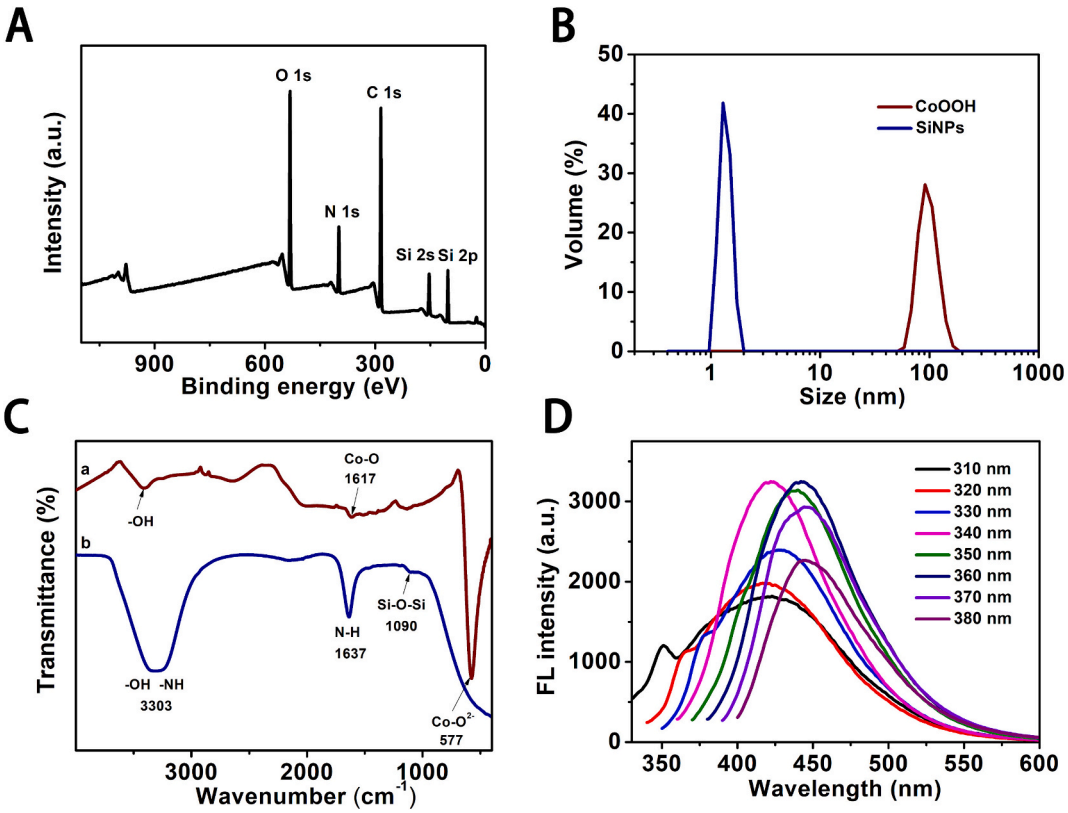

Fig. 2. (A) XPS full spectrum of SiNPs. (B) DLS particle size distributions of SiNPs and CoOOH nanoflakes. (C) FT-IR spectra of CoOOH nanoflakes (line a) and SiNPs (line b). (D) Fluorescence emission spectra of SiNPs with different excitation wavelengths (310, 320, 330, 340, 350, 360, 370 and 380 nm).

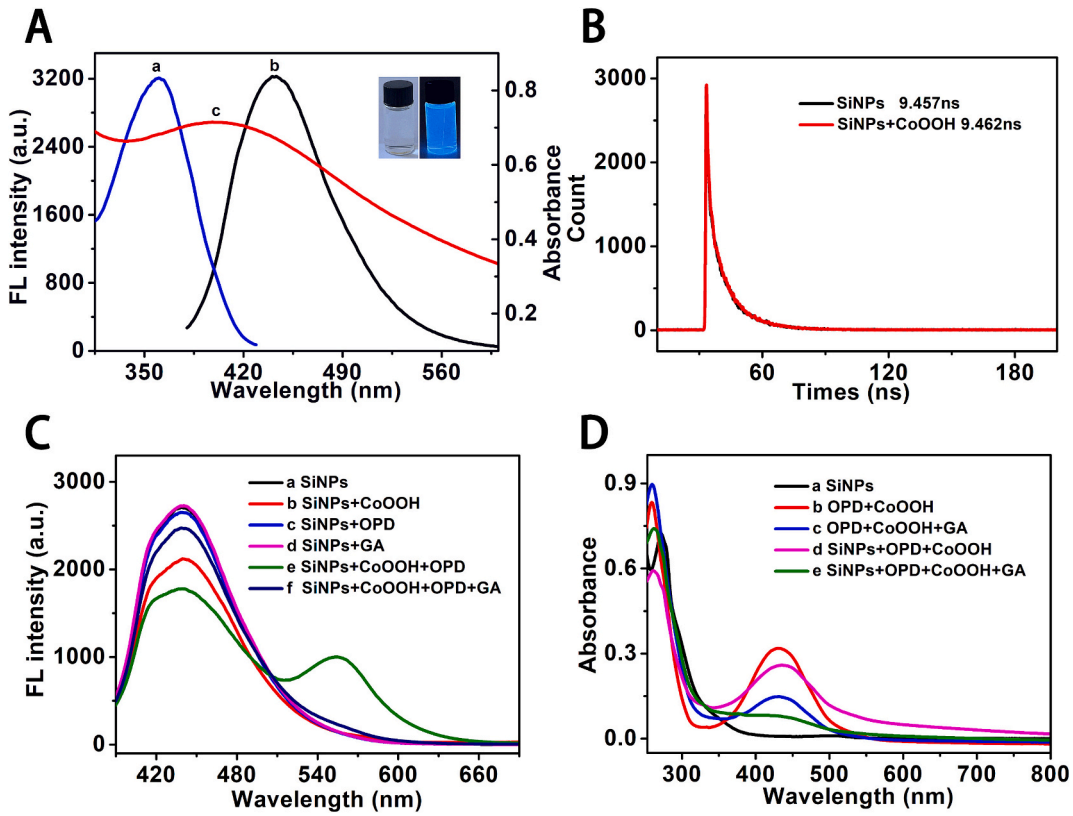

Fig. 3. (A) Fluorescent excitation (a, blue line) and emission (b, black line) spectra of SiNPs and UV–vis absorption spectra of CoOOH nanoflakes (c, red line). (B) The fluorescence lifetime of SiNPs in the absence and presence of CoOOH nanoflakes. (C) Fluorescence spectra of SiNPs (line a), SiNPs+CoOOH (line b), SiNPs+OPD (line c), SiNPs+GA (line d), SiNPs+CoOOH+OPD (line e), SiNPs+CoOOH+OPD + GA (line f). (D) UV–vis absorption spectra of SiNPs (line a), OPD + CoOOH (line b), OPD + CoOOH+GA (line c),SiNPs+CoOOH+OPD (line d), SiNPs+CoOOH+OPD + GA (line e).

2.4. The detection of gallic acid

150 μL of Britton-Robinson (BR) buffer (40 mM, pH = 6), 150 μL of CoOOH nanoflakes (0.1 mg·mL^{-1}), 150 μL of OPD (0.75 mM), different concentrations of GA and ultrapure water were mixed and diluted to 1.4 mL. The mixed solution was set at room temperature for 90 min. Then, 100 μL of SiNPs (Adjust pH to neutral using hydrochloric acid) was added into above solution. These fluorescence spectra were measured with excitation wavelength of 360 nm.

2.5. Foods samples analysis

The sample pretreatment methods refered to previous literature with minor modifications (Q. Tan et al., 2022). 0.5 g of green tea and red tea were soaked with boiling ultrapure water (10 mL) for three times and filtered with 0.22 μm filter membranes, respectively. The solution was transferred to 50 mL volumetric flask. Fruits and nut (lychee, apple, banana, grape, mango and chestnut) were cut up and crushed by food pulverizer. 5.0 g food samples were dispersed in 30 mL ultrapure water and ultrasound for 30 min, which transferred to 50 mL volumetric flask. These solutions were filtered by filter paper and centrifuged at 15000 rpm with 10 min.

These samples diluted to certain multiples and mixed with varying concentrations of standard GA solutions (0, 2.00 μM, 4.00 μM). After that, the following analysis of GA in food samples referred to above procedure in “2.4 The detection of gallic acid”.

3. Results and discussion

3.1. Characterization of materials

The SiNPs are selected as a fluorescence signal of probe, which have favorable photostability and outstanding fluorescence performance. The morphology of proposed SiNPs is characterized by transmission electron microscopy (TEM). The TEM image shows that SiNPs have obvious lattice fringes with average diameter of 4 nm (Fig. 1A), which is consistent with the hydrodynamic size observed in Fig. 2B. The XRD pattern of SiNPs demonstrates in Fig. S1, which also indicates the synthesis of SiNPs. TEM image in Fig. 1B demonstrates that flake-like CoOOH were successfully prepared, which are hexagonal with a length of 120 nm in accordance with hydrodynamic size of Fig. 2B. In order to confirm the synthesis of CoOOH nanoflakes further, scanning electron microscopy (SEM) image indicates the flake-like shape of CoOOH (Fig. 1C). Additionally, The SEM mapping and energy-dispersive spectrometry (EDS) of CoOOH nanoflakes (Fig. S2) also prove the presence of O and Co elements.

As depicted in Fig. 1D, the X-ray diffraction (XRD) pattern displays three diffraction major peaks at 2θ = 23.3°, 2θ = 45.5°and 2θ = 59.3°. These peaks are assigned to the (003), (012) and (015) lattice faces of CoOOH nanoflakes, respectively. Fig. 1E and Fig. 1F shows X-ray photoelectron spectroscopy (XPS) analysis of CoOOH nanoflakes. Fig. 1E is full spectrum of CoOOH nanoflakes, which indicates the presence of Co and O elements further. Co 2p spectrum of Fig. 1F displays two major peaks at 780.2 and 795.3 eV, which correspond to Co 2p3/2 and Co 2p1/2. Above two shakeup satellite peaks illustrate the oxidation state of Co (III). The spin-orbit splitting energy of two Co 2p peaks is 15.1 eV, which is matched well with previously report in literature (Yang & Wang, 2022).

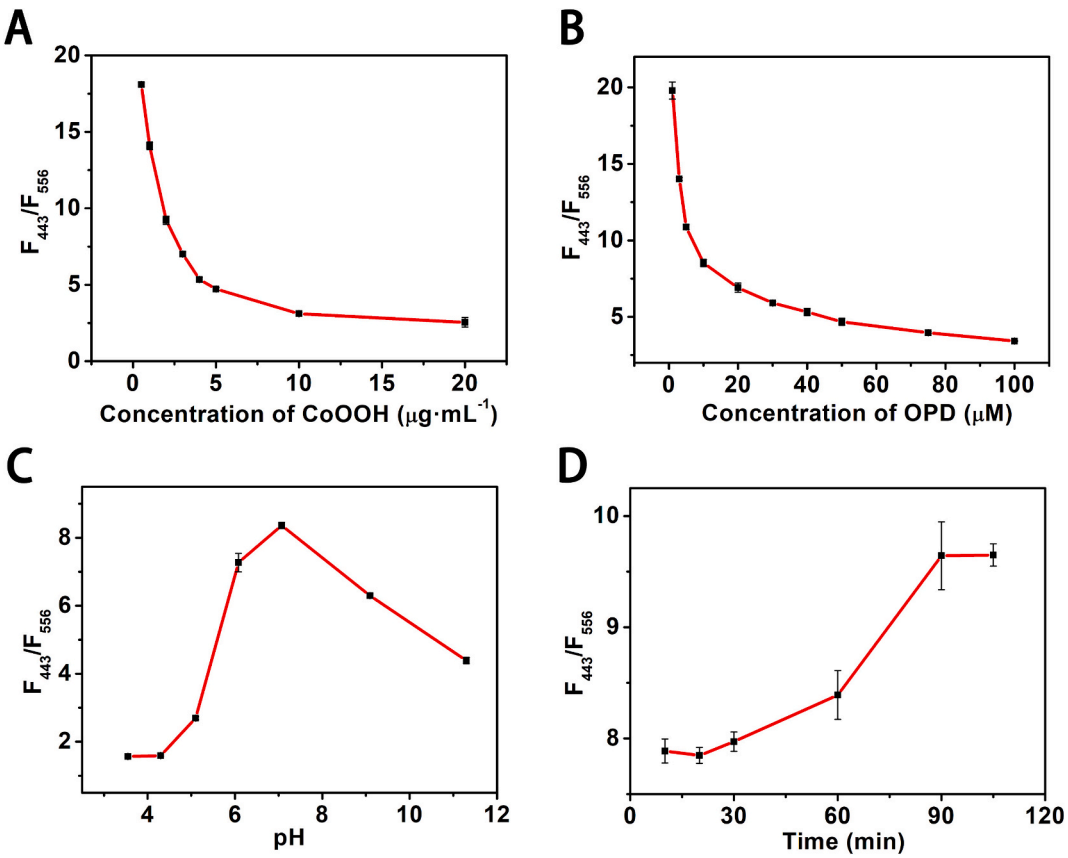

Fig. 4. (A) The effects of CoOOH nanoflakes concentrations, (B) The effects of OPD concentrations, (C) The effects of pH values, (D) The effects of reaction time.

3.2. *Spectral characterization and feasibility analysis*

The Fig. 2A is XPS full spectrum of SiNPs, which certifies the presence of C, O, N and Si elements. Furthermore, the high resolution XPS regions of Si 2 s, Si 2p, N 1 s and O 1 s for SiNPs were shown in Fig. S3. As depicted in Fig. 2B, the dynamic light scattering (DLS) results consist with TEM images of SiNPs and CoOOH nanoflakes sizes (Fig. 1A, B). These FT-IR spectra in Fig. 2C display the surface chemical structure of CoOOH nanoflakes and SiNPs, which proves successful preparation of nanomaterials. The FT-IR spectra analysis (line a, Fig. 2C) shows that CoOOH nanoflakes have characteristic absorption bands located at 577 cm^{-1} (Co—O^{2-}), 1617 cm^{-1} (Co—O) and 3303 cm^{-1} (—OH), which agree with previous literature (S. G. Liu et al., 2019). As shown in line b of SiNPs, the strong broad peak at 3303 cm^{-1} corresponds to stretching vibration of O—H bond and N—H bond, and the peak at 1637 cm^{-1} is related to the bending vibration of N—H bond. The slight peak (~1090 cm^{-1}) attributes to Si-O-Si asymmetric stretching vibration peak.

To explore the spectral properties of nanoparticles, emission wavelengths of SiNPs with different excitation wavelengths were recorded in Fig. 2D. The emission wavelength of SiNPs depends on an excitation wavelength of 310 to 380 nm with a slight red shift from 420 to 443 nm, which indicates the excitation-dependent property of SiNPs. The quantum yield of fluorescent silicon nanoparticles was calculated to be 12.34 %, which ensured excellent optical sensing and imaging.

In Fig. 3A, fluorescent excitation and emission spectra of SiNPs overlaps significantly with UV–vis absorption spectrum of CoOOH nanoflakes. In the previous report, CoOOH nanoflakes not only can be used as quencher, but also as peroxidase-like that can catalytically oxidizes OPD to generate fluorescent product DAP (Yang & Wang, 2022). The quenching mechanism would be fluorescent inner filter effect. The average fluorescent lifetime is calculated by the following equation, where τ_1 and τ_2 refer to fast and slow attenuation component, respectively.

$$\tau_{ave} = \left(\frac{A_1\tau_1^2 + A_2\tau_2^2}{A_1\tau_1 + A_2\tau_2}\right)$$

As demonstrated in Fig. 3B, fluorescence lifetime curves of SiNPs before (9.457 ns) and after adding CoOOH nanoflakes (9.462 ns) have no significant variation. Therefore, these results prove that quenching mechanism between SiNPs and CoOOH nanoflakes is inner filter effect. In addition, we measured zeta potential changes of CoOOH nanoflakes, SiNPs with and without adjusting pH to detection system in Fig. S4. The potential of CoOOH has an attraction with SiNPs in detection system, which further substantiates the possible interaction between them.

In order to confirm the feasibility of this probe for gallic acid detection, fluorescence emission and UV–vis absorption spectra response was performed. As depicted in Fig. 3C, fluorescence emission of SiNPs is not affected by OPD and GA (line c, line d). The SiNPs have a maximum fluorescence emission peak with 443 nm (line a) and fluorescent intensity would be quenched by CoOOH nanoflakes (line b). CoOOH nanoflakes can catalytically oxidize OPD to fluorescent DAP, which generate a new fluorescent emission peak with 556 nm (line e). Meanwhile, SiNPs' fluorescence emission peak (443 nm) decreases. When target analyte GA was added in the system, the fluorescence of SiNPs recovered and emission with 556 nm decreased, illustrating GA can reduce the produce of DAP (line f). As depicted in Fig. 3D, UV–vis absorption spectra were measured to testify the sensing mechanism. When OPD was added in the system, a broad absorption peak with 430 nm appeared (line b, line d). In the presence of GA, the absorption peak intensity (430 nm) significantly appeared to decline (line c, line e), which showed GA prevented OPD from being oxidized into DAP effectively (An et al., 2021).

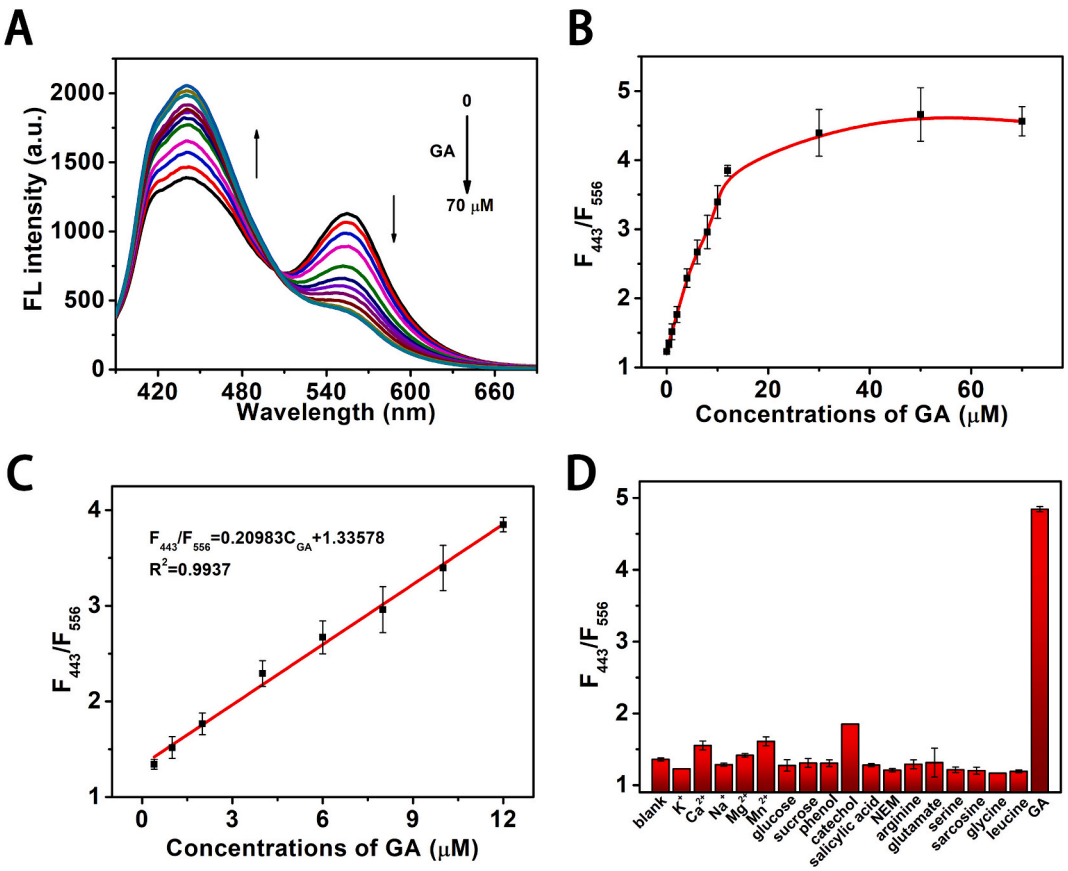

Fig. 5. (A) Fluorescence responses of nanoprobe (CoOOH/OPD/SiNPs) with various concentrations (0, 0.4, 1.0, 2.0, 4.0, 6.0, 8.0, 10, 12, 30, 50 and 70 μM) of GA under 360 nm excitation wavelength. (B) The corresponding response curve of F_{443}/F_{556} with GA concentrations under optimal conditions. (C) The linear relationship of F_{443}/F_{556} against the GA concentration (0.4, 1.0, 2.0, 4.0, 6.0, 8.0, 10 and 12 μM). (D) Selectivity of CoOOH/OPD/SiNPs system for GA detection (interferences and target objects from left to right: blank, K^+, Ca^{2+}, Na^+, Mg^{2+}, Mn^{2+}, glucose, sucrose, phenol, catechol, salicylic acid, NEM, arginine, glutamate, serine, sarcosine, glycine, leucine and GA; concentrations: 70 μM).

3.3. Experimental parameters optimization

In order to acquire optimal response for GA detection, experimental conditions such as concentration of CoOOH, amount of OPD, pH and incubation time were explored. As shown in Fig. 4A, as the addition of CoOOH nanoflakes, F_{443}/F_{556} (the fluorescence intensity ratio of SiNPs at 443 nm and DAP at 556 nm) declined and reached a stable status. Hence, 10 $\mu g \cdot mL^{-1}$ of CoOOH nanoflakes was selected for next procedure. Meanwhile, the concentration of OPD have similar variation trend (Fig. 4B). With the OPD amount increasing, emission peak at 556 nm (DAP) increased gradually. Thus, F_{443}/F_{556} decreased and 75 μM was chosen for optimal OPD concentration.

The pH values have great effects on sensitivity and liner range. In Fig. S5, pH values have little effect on fluorescence intensity of SiNPs. As exhibited in Fig. 4C, F_{443}/F_{556} reaches the maximum at pH 7.0. However, pH 6.0 was selected for gallic acid detection. The Fig. S6 shows the fluorescence response of probe for GA and blank sample at pH 7.0 and 6.0. We discovered a high F_{443}/F_{556} ratio between pH 6.0 and blank sample compared with pH 7.0. Therefore, pH value is selected as pH 6.0 properly. In addition, the incubation time is illustrated in Fig. 4D. The value of F_{443}/F_{556} remains stable after 90 min. Therefore, 90 min is chosen as optimal reaction time for gallic acid detection. In order to evaluate the stability of nanoprobe, different reaction time were performed to gallic acid and blank samples detection (Fig. S7). This detection method has an excellent stability within 24 h.

Table 1
Results of gallic acid in different tea, fruits and nut with proposed nanoprobe.

Samples	Spiked (μM)	Found (μM)	Recovery (%)	RSD (%, $n = 3$)
Green tea	0	2.52 ± 0.13	–	2.43
	2.00	4.85 ± 0.10	107.3	3.09
	4.00	6.84 ± 0.22	104.9	4.50
	0	0.54 ± 0.03	–	0.90
	2.00	2.79 ± 0.13	109.8	2.56
Red tea	4.00	4.74 ± 0.01	104.4	0.36
Lychee	0	0.32 ± 0.05	–	0.94
	2.00	2.25 ± 0.27	97.0	5.09
	4.00	3.83 ± 0.21	88.7	3.88
Apple	0	–	–	–
	2.00	2.08 ± 0.09	103.9	1.57
	4.00	3.58 ± 0.04	90.1	0.64
Banana	0	0.30 ± 0.03	–	0.58
	2.00	2.39 ± 0.20	103.9	3.86
	4.00	4.56 ± 0.13	106.0	2.33
Grape	0	–	–	–
	2.00	2.19 ± 0.20	109.4	2.57
	4.00	3.66 ± 0.06	91.5	1.09
Mango	0	1.33 ± 0.18	–	3.32
	2.00	3.60 ± 0.10	108.2	1.77
	4.00	5.18 ± 0.19	97.2	3.77
Chestnut	0	0.47 ± 0.11	–	2.00
	2.00	2.60 ± 0.12	105.1	2.39
	4.00	4.66 ± 0.15	104.0	2.95

Table 2
Comparison of gallic acid detection with previous reported various methods.

Materials	Methods	Linearty (μM)	LOD (μM)	References
Modified ESM	Electrochemistry	5–65	1.707	(Datta, Kanjilal, & Sarkar, 2017)
Fe-N-C/AuNPs/GCE	Electrochemistry	5–500	1.284	(Zhang et al., 2023)
Perovskite $LaFeO_3$	Colorimetry	0.6–36	0.4	(Chen et al., 2020)
TMB/H_2O_2/Fe^{2+}	Colorimetry	0–60	0.8	(Qi, Ding, Lu, & Wang, 2023)
$NaErF_4$: Tm@SiO_2@ZIF-8	Fluorescence	0–30	0.35	(Zhang et al., 2021)
TMB/H_2O_2/Fe^{2+}	Fluorescence	0–80	0.31	(Qi et al., 2023)
CoOOH/OPD/SiNPs	Ratio fluorescence	0.4–12	0.16	this work

3.4. Detection of gallic acid in solution and food samples

As depicted in Fig. 5A, under optimized experimental conditions, the fluorescence peak at 443 nm (SiNPs) increases whereas 556 nm (DAP) declines gradually with rising GA concentrations (0–70 μM). The dependence of fluorescence ratio (F_{443}/F_{556}) with GA concentrations is displayed in Fig. 5B. As the concentration of GA increased, F_{443}/F_{556} enhanced and reached equilibrium. As shown in Fig. 5C, an excellent linear relationship ($R^2 = 0.9937$) is acquired between fluorescence ratio (F_{443}/F_{556}) and GA concentration in the range of 0.4–12 μM. The linear equation is $F_{443}/F_{556} = 0.20983C_{GA} + 1.33578$. This method gains a low detection limit (LOD) of 0.16 μM according to 3σ/k principle, where *k* and σ represent the slope of calibration line and standard deviation of blank samples, respectively. In Fig. 5D, in order to evaluate selectivity of GA detection, we examined several potential interfering substances, such as ions, saccharides, phenols, amino acid and others etc. These results of nanoprobe shows high selectivity toward gallic acid detection.

The novel nanoprobe was applied to gallic acid detection in aqueous solution and different kinds of tea leaves, fruits and nut. In order to illustrate the feasibility of this nanoprobe, analysis results before and after standard addition of GA in green tea, red tea, lychee, apple, banana, grape, mango and chestnut were listed in Table 1. The recoveries ranged from 104.9 to 107.3 % with relative standard deviations (RSDs) over the range of 2.43–4.50 % in green tea. Meanwhile, the recoveries were 104.4–109.8 % with RSDs of 0.36–2.56 % in red tea. The recovery rate of gallic acid in lychee, apple, banana, grape, mango and chestnut was 88.7–97.0 %, 90.1–103.9 %, 103.9–106.0 %, 91.5–109.4 %, 97.2–108.2 % and 104.0–105.1 %, respectively. It is meaningful that the proposed probe has potential for gallic acid quantification in real samples with excellent practicability and repeatability. Moreover, a comparison for GA detection with proposed probe and previously reported various methods was made (Table 2). These results demonstrate that LOD of the nanoprobe is comparable with or superior to some previously reported methods.

4. Conclusion

Summarily, a novel fluorescent silicon nanoparticles-based ratiometric fluorescent nanoprobe (named CoOOH/OPD/SiNPs) was established for the detection of gallic acid. The fluorescence of SiNPs (443 nm) would be quenched by CoOOH nanoflakes and OPD was oxidized to DAP (556 nm). Simultaneously, SiNPs' fluorescence is quenched by DAP due to inner filter effect. With the addition of gallic acid, due to peroxidase-like activity of CoOOH nanoflakes, CoOOH decomposed and declined the generation of DAP, causing IFE being inhibited and realizing gallic acid detection. Hence, the nanoprobe enables gallic acid detection in water, tea leaves, fruits and nut fruits, which has potential application for complicated substances analysis on site.

CRediT authorship contribution statement

Chunlei Yang: Writing – review & editing, Writing – original draft, Methodology, Investigation, Funding acquisition. **Guiju Xu:** Writing – review & editing, Supervision. **Chenghao Hou:** Supervision. **Hongwei Zhang:** Supervision, Project administration.

Declaration of competing interest

The authors declare that they have no known competing financial interests or personal relationships that could have appeared to influence the work reported in this paper.

Data availability

No data was used for the research described in the article.

Acknowledgements

This research was financially supported by Natural Science Foundation of Shandong Province of China (No. ZR2023QC284), Agricultural Science and Technology Innovation Project of Shandong Academy of Agricultural Sciences (No. CXGC2024F09).

Appendix A. Supplementary data

Supplementary data to this article can be found online at https://doi.org/10.1016/j.fochx.2024.101843.

References

An, X., Chen, R., Chen, Q., Tan, Q., Pan, S., Liu, H., & Hu, X. (2021). A MnO_2 nanosheet-assisted ratiometric fluorescence probe based on carbon quantum dots and o-phenylenediamine for determination of 6-mercaptopurine. *Microchimica Acta, 188* (5), 156. https://doi.org/10.1007/s00604-021-04802-4

Badea, M., di Modugno, F., Floroian, L., Tit, D. M., Restani, P., Bungau, S., & Aleya, L. (2019). Electrochemical strategies for gallic acid detection: Potential for application in clinical, food or environmental analyses. *Science of the Total Environment, 672*, 129–140. https://doi.org/10.1016/j.scitotenv.2019.03.404

Baghayeri, M., Amiri, A., Hasheminejad, E., & Mahdavi, B. (2018). Poly(aminohippuric acid)–sodium dodecyl sulfate/functionalized graphene oxide nanocomposite for amplified electrochemical sensing of gallic acid. *Journal of the Iranian Chemical Society, 15*(9), 1931–1938. https://doi.org/10.1007/s13738-018-1390-3

Boye, B., Brillas, E., Buso, A., Farnia, G., Flox, C., Giomo, M., & Sandonà, G. (2006). Electrochemical removal of gallic acid from aqueous solutions. *Electrochimica Acta, 52*(1), 256–262. https://doi.org/10.1016/j.electacta.2006.04.062

Chen, L., Yang, J., Chen, W., Sun, S., Tang, H., & Li, Y. (2020). Perovskite mesoporous $LaFeO_3$ with peroxidase-like activity for colorimetric detection of gallic acid. *Sensors and Actuators B: Chemical, 321*, Article 128642. https://doi.org/10.1016/j.snb.2020.128642

Datta, S., Kanjilal, B., & Sarkar, P. (2017). Electrochemical sensor for detection of polyphenols in tea and wine with differential pulse voltammetry and electrochemical impedance spectroscopy utilizing tyrosinase and gold nanoparticles decorated biomembrane. *Journal of the Electrochemical Society, 164*(4), B118. https://doi.org/10.1149/2.0971704jes

Dhalwal, K., Shinde, V. M., Biradar, Y. S., & Mahadik, K. R. (2008). Simultaneous quantification of bergenin, catechin, and gallic acid from Bergenia ciliata and Bergenia ligulata by using thin-layer chromatography. *Journal of Food Composition and Analysis, 21*(6), 496–500. https://doi.org/10.1016/j.jfca.2008.02.008

Dmitrienko, S. G., Medvedeva, O. M., Ivanov, A. A., Shpigun, O. A., & Zolotov, Y. A. (2002). Determination of gallic acid with 4-nitrobenzenediazonium tetrafluoroborate by diffuse reflectance spectrometry on polyurethane foam. *Analytica Chimica Acta, 469*(2), 295–301. https://doi.org/10.1016/S0003-2670(02)00715-8

Dou, Y.-K., Chen, Y., He, X.-W., Li, W.-Y., Li, Y.-H., & Zhang, Y.-K. (2017). Synthesis of water-dispersible Mn^{2+} functionalized silicon nanoparticles under room temperature and atmospheric pressure for fluorescence and magnetic resonance dual-modality imaging. *Analytical Chemistry, 89*(21), 11286–11292. https://doi.org/10.1021/acs.analchem.7b01644

Huang, X., Song, J., Yung, B. C., Huang, X., Xiong, Y., & Chen, X. (2018). Ratiometric optical nanoprobes enable accurate molecular detection and imaging. *Chemical Society Reviews, 47*(8), 2873–2920. https://doi.org/10.1039/C7CS00612H

Jiménez-Prieto, R., Silva, M., & Pérez-Bendito, D. (1996). Simultaneous determination of gallic acid and resorcinol based on an oscillating chemical reaction by the analyte pulse perturbation technique. *Analytica Chimica Acta, 334*(3), 323–330. https://doi.org/10.1016/S0003-2670(96)00346-7

Li, M., Fan, J., Li, H., Du, J., Long, S., & Peng, X. (2018). A ratiometric fluorescence probe for lysosomal polarity. *Biomaterials, 164*, 98–105. https://doi.org/10.1016/j.biomaterials.2018.02.044

Li, S., Sun, H., Wang, D., Qian, L., Zhu, Y., & Tao, S. (2012). Determination of gallic acid by flow injection analysis based on luminol-$AgNO_3$-Ag NPs chemiluminescence system. *Chinese Journal of Chemistry, 30*(4), 837–841. https://doi.org/10.1002/cjoc.201100160

Liang, Z., Zhai, H., Chen, Z., Wang, H., Wang, S., Zhou, Q., & Huang, X. (2016). A simple, ultrasensitive sensor for gallic acid and uric acid based on gold microclusters/sulfonate functionalized graphene modified glassy carbon electrode. *Sensors and Actuators B: Chemical, 224*, 915–925. https://doi.org/10.1016/j.snb.2015.10.101

Liu, H. X., Liu, Q., Zhang, X. Y., Huan, Y. F., Wang, L. T., Ye, K. Q., & Yue, H. J. (2014). Determination of gallic acid content in terminalia by capillary zone electrophoresis. *Advanced Materials Research, 850-851*, 1275–1278. https://doi.org/10.4028/www.scientific.net/AMR.850-851.1275

Liu, S. G., Han, L., Li, N., Fan, Y. Z., Yang, Y. Z., Li, N. B., & Luo, H. Q. (2019). A ratiometric fluorescent strategy for alkaline phosphatase activity assay based on g-C_3N_4/CoOOH nanohybrid via target-triggered competitive redox reaction. *Sensors and Actuators B: Chemical, 283*, 515–523. https://doi.org/10.1016/j.snb.2018.12.052

Niu, X., Pei, W.-Y., Ma, J.-C., Yang, J., & Ma, J.-F. (2022). Simultaneous electrochemical detection of gallic acid and uric acid with p-tert-butylcalix[4]arene-based coordination polymer/mesoporous carbon composite. *Microchimica Acta, 189*(3), 93. https://doi.org/10.1007/s00604-022-05201-z

Pan, L., Li, X., Zhang, Q., Xu, S., Yang, L., Yang, F., & Jiang, C. (2022). A boric acid functional multi-emission metal organic frameworks-based fluorescence sensing platform for visualization of gallic acid. *Chemical Engineering Journal, 450*, Article 138283. https://doi.org/10.1016/j.cej.2022.138283

Pang, S., & Liu, S. (2020). Dual-emission carbon dots for ratiometric detection of Fe^{3+} ions and acid phosphatase. *Analytica Chimica Acta, 1105*, 155–161. https://doi.org/10.1016/j.aca.2020.01.033

Peng, F., Su, Y., Zhong, Y., Fan, C., Lee, S.-T., & He, Y. (2014). Silicon nanomaterials platform for bioimaging, biosensing, and cancer therapy. *Accounts of Chemical Research, 47*(2), 612–623. https://doi.org/10.1021/ar400221g

Qi, L., Ding, H., Lu, C., & Wang, X. (2023). A dual-mode optical assay for iron(II) and gallic acid based on Fenton reaction. *Luminescence, 38*(7), 1167–1174. https://doi.org/10.1002/bio.4247

Sekar, S., Huijun, J., Liuzhu, Z., Jin, C., Lee, S., Kim, D. Y., & Manikandan, R. (2022). Copper phthalocyanine conjugated graphitic carbon nitride nanosheets as an efficient electrocatalyst for simultaneous detection of natural antioxidants. *Electrochimica Acta, 413*, Article 140150. https://doi.org/10.1016/j.electacta.2022.140150

Shahamirifard, S. A., Ghaedi, M., Razmi, Z., & Hajati, S. (2018). A simple ultrasensitive electrochemical sensor for simultaneous determination of gallic acid and uric acid in human urine and fruit juices based on zirconia-choline chloride-gold nanoparticles-modified carbon paste electrode. *Biosensors and Bioelectronics, 114*, 30–36. https://doi.org/10.1016/j.bios.2018.05.009

Stanković, D. M., Ognjanović, M., Martin, F., Švorc, Ľ., Mariano, J. F. M. L., & Antić, B. (2017). Design of titanium nitride- and wolfram carbide-doped RGO/GC electrodes for determination of gallic acid. *Analytical Biochemistry, 539*, 104–112. https://doi.org/10.1016/j.ab.2017.10.018

Švecová, B., Bordovská, M., Kalvachová, D., & Hájek, T. (2015). Analysis of Czech meads: Sugar content, organic acids content and selected phenolic compounds content. *Journal of Food Composition and Analysis, 38*, 80–88. https://doi.org/10.1016/j.jfca.2014.11.002

Tan, Q., An, X., Pan, S., Zhen, S., Hu, Y., & Hu, X. (2022). A facile and sensitive ratiometric fluorescent sensor for determination of gallic acid. *Microchemical Journal, 172*, Article 106922. https://doi.org/10.1016/j.microc.2021.106922

Tan, X., Li, Q., & Yang, J. (2020). CdTe QDs based fluorescent sensor for the determination of gallic acid in tea. *Spectrochimica Acta Part A: Molecular and Biomolecular Spectroscopy, 224*, Article 117356. https://doi.org/10.1016/j.saa.2019.117356

Wang, L., Liu, Y., Yang, Z., Wang, Y., Rao, H., Yue, G., … Wang, X. (2020). A ratiometric fluorescence and colorimetric dual-mode assay for H_2O_2 and xanthine based on Fe, N co-doped carbon dots. *Dyes and Pigments, 180*, Article 108486. https://doi.org/10.1016/j.dyepig.2020.108486

Wang, X., Tan, W., Wang, Y., Wu, D., & Kong, Y. (2019). Electrosynthesis of poly(m-phenylenediamine) on the nanocomposites of palygorskite and ionic liquid for electrocatalytic sensing of gallic acid. *Sensors and Actuators B: Chemical, 284*, 63–72. https://doi.org/10.1016/j.snb.2018.12.133

Wu, Z., Nan, D., Yang, H., Pan, S., Liu, H., & Hu, X. (2019). A ratiometric fluorescence-scattered light strategy based on MoS_2 quantum dots/CoOOH nanoflakes system for ascorbic acid detection. *Analytica Chimica Acta, 1091*, 59–68. https://doi.org/10.1016/j.aca.2019.09.054

Xing, K., Ge, J., Wang, W.-X., Geng, X., Shen, X.-P., Tang, J.-L., & Li, Z.-H. (2019). A turn-on fluorescent probe for sensitive detection of ascorbic acid based on SiNP–MnO_2 nanocomposites. *New Journal of Chemistry, 43*(24), 9466–9471. https://doi.org/10.1039/C9NJ02106J

Xu, W., Chen, J., Sun, S., Tang, Z., Jiang, K., Song, L., … Lin, H. (2018). Fluorescent and photoacoustic bifunctional probe for the detection of ascorbic acid in biological fluids, living cells and in vivo. *Nanoscale, 10*(37), 17834–17841. https://doi.org/10.1039/C8NR03435D

Xu, X., He, L., Long, Y., Pan, S., Liu, H., Yang, J., & Hu, X. (2019). S-doped carbon dots capped ZnCdTe quantum dots for ratiometric fluorescence sensing of guanine. *Sensors and Actuators B: Chemical, 279*, 44–52. https://doi.org/10.1016/j.snb.2018.09.102

Yang, C., Gao, N., Liu, Y., Zhao, H., Jing, J., & Zhang, X. (2021). A silicon nanoparticle-based nanoprobe for ratiometric fluorescence and visual detection of glucose. *New Journal of Chemistry, 45*(41), 19515–19520. https://doi.org/10.1039/D1NJ03826E

Yang, X. P. Z. W. X., & Wang, J.-H. (2022). CoOOH nanosheets ensure ratiometric fluorescence assay of acetylcholinesterase. *Talanta, 249*, Article 123664. https://doi.org/10.1016/j.talanta.2022.123664

Zhang, W., Li, X., Hu, X., Li, C., Liu, S., Ma, J., & Wang, Z. (2023). A novel electrochemical sensor based on an Fe–N–C/AuNP nanohybrid for rapid and sensitive gallic acid detection. *New Journal of Chemistry, 47*(13), 6448–6456. https://doi.org/10.1039/D3NJ00345K

Zhang, X., Chen, X., Kai, S., Wang, H.-Y., Yang, J., Wu, F.-G., & Chen, Z. (2015). Highly sensitive and selective detection of dopamine using one-pot synthesized highly photoluminescent silicon nanoparticles. *Analytical Chemistry, 87*(6), 3360–3365. https://doi.org/10.1021/ac504520g

Zhang, X.-P., Zhao, C.-X., Shu, Y., & Wang, J.-H. (2019). Gold nanoclusters/iron oxyhydroxide platform for ultrasensitive detection of butyrylcholinesterase. *Analytical Chemistry, 91*(24), 15866–15872. https://doi.org/10.1021/acs.analchem.9b04304

Zhang, Y., Ning, L., Gao, D., Jia, D., Gu, W., & Liu, X. (2021). A highly sensitive upconversion nanoparticles@zeolitic imidazolate frameworks fluorescent nanoprobe for gallic acid analysis. *Talanta, 233*, Article 122588. https://doi.org/10.1016/j.talanta.2021.122588